Materials Advances

ROYAL SOCIETY OF CHEMISTRY

PAPER

View Article Online
View Journal | View Issue

Cite this: *Mater. Adv.*, 2025, 6, 6130

Side-chain engineering of semiconducting polymers with poly(benzyl ether) dendrons: impact on electronic and mechanical properties†

Gage T. Mason,[a] Chloé Lisowski,[a] Piumi Kulatunga,[a] Tiago C. Gomes,[a] Angela Awada,[a] Yu-Xin Hsu,[b] Yu-Cheng Chiu[b] and Simon Rondeau-Gagné*[a]

The rise of organic electronics is unlocking exciting possibilities for the development of flexible, sustainable, and energy-efficient technologies. From wearable devices and intelligent food packaging to light-harvesting materials and smart textiles, these innovations are driving the next establishment of the Internet of Things (IoT) and other AI-driven autonomous systems, where interconnected devices and intelligent technologies seamlessly work together to transform industries and daily life. At the core of these emerging technologies are semiconducting polymers, which offer a unique combination of synthetic tunability, solution processability, and tuneable optoelectronic and mechanical properties. These features pave the way for cutting-edge fabrication techniques—such as 3D and inkjet printing—to create high-performance devices. Achieving solution processability in these polymer systems often requires the incorporation of bulky, acyclic aliphatic side chains, amongst many others, to enhance solubility and mitigate strong molecular aggregation. These side chains can significantly impact multiple properties, including charge carrier mobility through their influence on the polymer nanostructure in thin films. This work explores the utilization of dendronized side chains to modulate the properties of semicrystalline polymers. More precisely, we developed a new series of materials by integrating high-performance diketopyrrolopyrrole (DPP)-based backbones with two distinct poly(benzyl ether) side chains and two different donor units. These structural variations were found to significantly influence processing conditions, as well as the electronic and thermomechanical properties of the resulting polymers. Comprehensive characterization, including grazing incidence wide-angle X-ray scattering (GIWAXS), atomic force microscopy (AFM), quantitative nanomechanical mapping (for Young's moduli), and dynamic mechanical analysis (DMA) to determine glass transitions, was performed. The polymers were subsequently employed in the fabrication of organic field-effect transistors (OFETs) to study their impact on the electronic properties. The incorporation of novel dendron-like side chains provides a promising strategy for advancing side-chain engineering in semiconducting polymers, offering new avenues in the development of emerging printed organic electronics.

Received 6th May 2025,
Accepted 11th July 2025

DOI: 10.1039/d5ma00446b

rsc.li/materials-advances

Introduction

The rapid advancement of organic electronics, where organic electroactive materials are developed and processed into cutting-edge technologies, is opening exciting new pathways for flexible, sustainable, energy-efficient, integrable devices.[1–5] This progress is particularly evident in the Internet of Things (IoT), where an interconnected network of smart devices—often low-cost sensors—is deployed across diverse objects and individuals for various applications.[6,7] These range from monitoring food supplies and environmental conditions in air and water to tracking the status of packaged goods and human health.[8–10] At the intersection of computer science and electronics, organic electronics has enabled the creation of lightweight, flexible, and cost-effective electronic devices that could become the hardware backbone for AI-driven applications and autonomous systems, such as wearable devices, light-harvesting solar technologies, intelligent food packaging, smart textiles, and biosensors.[2,11–16] While these technologies evolve rapidly, the materials used to fabricate them are critical to their performance and applicability. Among the key material properties required to advance these

[a] *Department of Chemistry and Biochemistry, University of Windsor, 401 Sunset Avenue, Windsor, ON N9B 3P4, Canada. E-mail: srondeau@uwindsor.ca*
[b] *Department of Chemical Engineering, National Taiwan University of Science and Technology, No. 43 Keelung Road, Sec 4, Taipei 10607, Taiwan*

† Electronic supplementary information (ESI) available: Detailed experimental procedures for all new compounds and a complete characterization of materials and devices. See DOI: https://doi.org/10.1039/d5ma00446b

technologies, electronic and mechanical performance are particularly vital for achieving high-performing yet soft and adaptable devices that can integrate seamlessly into complex and varied form factors.[1,17–20]

Within this growing materials toolbox, semiconducting polymers stand out due to their unique properties. These materials offer tunability, solution processability, and the ability to customize their properties through rational design.[21] This enables precise control over thermomechanical properties, such as low Young's moduli and glass transition temperatures (T_g), which are crucial for achieving flexibility and durability.[1,20,22] These features position semiconducting polymers as ideal candidates for the large-scale manufacturing of printed electronics, pushing the boundaries of what these emerging technologies can achieve.[10,14,23,24]

Among the various synthetic strategies for fine-tuning and optimizing semiconducting polymers, side-chain engineering stands out as particularly effective.[21] Often employed to solubilize otherwise insoluble π-conjugated polymers, side chains have evolved into critical design elements that significantly influence key properties such as solid-state polymer chain packing, polarity, aggregation, and thermal transitions.[21,25–27] Numerous studies, predominantly using long branched aliphatic chains, demonstrate how side chains can be precisely tailored to control and enhance the performance of materials in organic electronics. For example, Bao *et al.* reported a series of branched aliphatic side chains with different lengths in diketopyrrolopyrrole-based (DPP) polymers and found that the morphology (face-on *vs.* edge-on orientation) changes drastically with the side chain length. They also found that these morphological changes lead to drastic differences in charge carrier mobility, ranging between 1.4 and 3.7 $cm^2 V^{-1} s^{-1}$.[28] Their findings suggest that a mixed morphology is highly beneficial for creating charge percolation pathways and an intertwined 3-D network. Beyond traditional alkyl chains, side chains in semiconducting polymers provide versatile anchor points to push functionality further. Precise design of new side chains has enabled the incorporation of a diverse range of complex moieties and functional groups, including ethylene glycol, carbohydrates, amino acids, cross-linkable groups, oligosiloxanes and more.[29–34] These advancements in side chain engineering were shown to not only lead to drastically different physical and chemical properties but also broaden the application potential of conjugated polymers in next-generation electronic devices.

Notably, as demonstrated in numerous examples of side chain engineering, the bulk dimension and molecular flexibility of these solubilizing side chains are key design elements that show a profound influence on the electronic and mechanical properties of semiconducting polymers. For instance, Mei *et al.* reported the use of bulky oligosiloxane side chains in polyisodingo polymers.[35] In this work, the authors showed that pushing the siloxane chains further away from the backbone led to an important decrease in π-stacking distances, from 3.63 to 3.37 Å. This difference also led to an important increase in device performance, reaching a charge carrying mobility as high as 4.8 $cm^2 V^{-1} s^{-1}$ in OFETs. This phenomenon can be attributed to the bulkiness of these side chains: as the side chain gets bulkier and pushed further away from the main polymer chain, the π-conjugated backbone can get closer through enhanced π-stacking, thus promoting charge transport through charge hopping and the overall charge carrier mobility measured in thin film transistors, all while remaining processable. Building from this finding, several reports focused on the rational design of side chains to increase their bulkiness and investigated not only the impact on the electronic properties but also the impact on the mechanical properties. For instance, Chen *et al.* prepared a series of isoindigo–bithiophene polymers with systematically varying carbosilane side chain lengths (from C6 to C10) and found that as longer side chains were incorporated into the polymers the film moduli decreased, and that the longest chain maintained the highest charge carrier mobility under strain.[36]

Building on previous work, the incorporation of dendron-inspired side chains into semiconducting polymers has been explored, with dendronized side chains emerging as a promising platform for advanced semiconductors. These side chains are distinguished by their high degree of functionalization, monodispersity, and bulkiness. Among others, the use of poly(benzyl ether) dendrons to modify conjugated polymers is a particularly attractive strategy that has been explored in polyphenylene and polythiophene-based conjugated polymers primarily to improve solubility and processability, though often at the cost of molecular packing and crystallinity.[37–39] Leveraging the unique features of dendronized side chains, our group developed a method to integrate short, polyamidoamine (PAMAM) dendritic side chains into semicrystalline diketopyrrolopyrrole-based polymers using an azide–alkyne Huisgen 1,3-dipolar cycloaddition reaction.[40] Comprehensive characterization of the resulting dendronized semiconducting polymers revealed that dendritic side chains effectively reduce polymer aggregation and crystallinity in thin films. Notably, PAMAM-containing polymers exhibited good charge transport properties in OFETs, performing in a similar manner to diketopyrrolopyrrole-based polymers featuring branched alkyl side chains. While these findings highlight the potential of dendritic side chains for designing advanced semiconducting polymers, their use remains relatively underexplored in semicrystalline donor–acceptor (D–A) semiconducting polymers, with their impact on optoelectronic, thermomechanical, and solid-state properties still challenging to predict. Exploring dendritic side chains derived from more rigid and bulky moieties, as well as their integration into D–A systems, is therefore an interesting avenue to explore more efficient organic electronics.

Herein, we report the design and synthesis of diketopyrrolopyrrole-based semiconducting polymers incorporating poly(benzyl ether) side chains (Fig. 1). Using a macromonomer approach, the dendritic side chain was expanded from generation 1 (**G1**) to generation 2 (**G2**) to investigate the effects of side chain bulkiness and rigidity on material properties. Additionally, the donor unit in the donor–acceptor polymers was changed from bithiophene to thienothiophene to explore the influence of donor design. Comprehensive characterization using optical spectroscopies, atomic force microscopy (AFM), and X-ray scattering revealed that the bulky dendronized side chains effectively

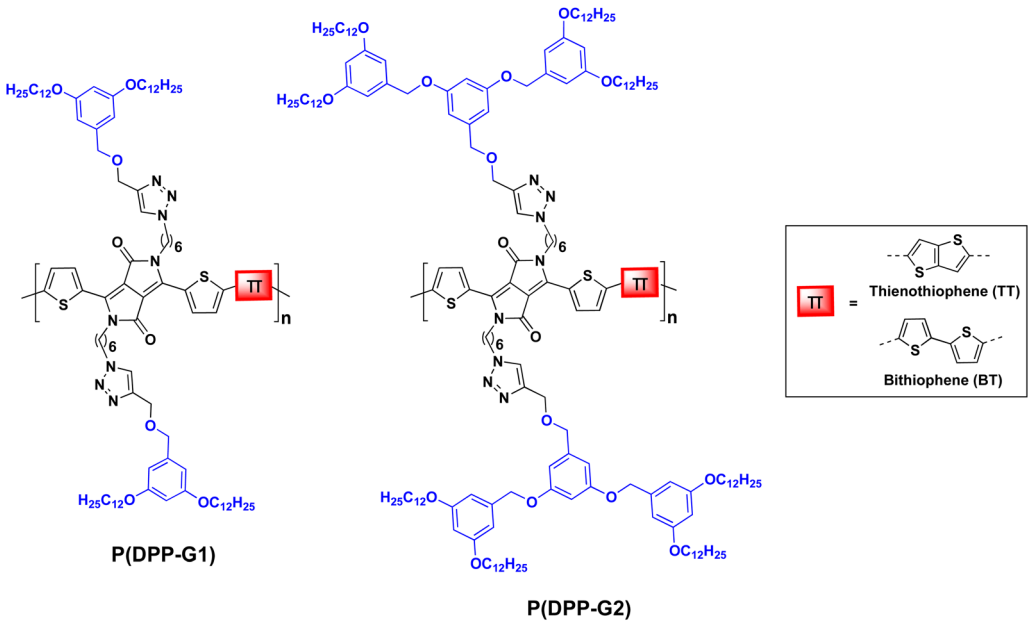

Fig. 1 Diketopyrrolopyrrole-based semiconducting polymers with dendritic poly(benzyl ether) side chains.

reduce polymer aggregation in solution while increasing interchain spacing in the solid state. Thermomechanical properties were analyzed using dynamic mechanical analysis (DMA) and quantitative nanomechanical mapping (AFM). The results showed that the side chain T_g is between −75 and −85 °C, while backbone T_g remains near 0 °C. Increasing the side chain generation from **G1** to **G2** softened the side chains, lowering the T_g, while the backbone T_g increased with side chain bulk. Similarly, the Young's moduli decreased with higher side chain generation, highlighting the influence of dendritic architecture on mechanical properties. Finally, the materials were tested in OFETs, revealing that increasing the size of the side chain incorporated into the polymer led to reduced charge carrier mobility but resulted in a softer material. Overall, these findings demonstrate the potential of incorporating bulky, non-traditional moieties using side chain engineering as a powerful strategy to tailor the nanoscale morphology, optoelectronic properties, and thermomechanical behavior of semiconducting polymers for softer organic electronic applications. At the same time, our results underscore the critical need for thoughtful side chain design and moiety selection, as excessive side chain bulk can disrupt thin film morphology, hinder molecular packing, and ultimately compromise electronic performance.

Results and discussion

The new DPP-based polymers with poly(benzyl ether) dendronized side chains are depicted in Fig. 1, with the synthetic procedure detailed in the ESI† (Schemes S1–S3). Poly(benzyl ether) dendrons were chosen as design elements for several reasons. First, the alkoxy chains within these dendrons can help maintain the solubility of the conjugated polymers in common organic solvents. Additionally, the multiple aryl groups of the dendrons can make the side chains significantly bulkier compared to typical alkyl chains, providing an ideal platform to evaluate the impact of these designs on key polymer properties. Lastly, the bulky nature of these dendrons is expected to hinder efficient polymer packing in the solid state, increasing the amorphous nature of the polymers and resulting in intrinsically softer materials. To synthesize the polymers, a macromonomer approach was employed to maximize functionalization and minimize defects. To investigate the impact of dendron generation on polymer properties, two specific side chain precursors (**G1** and **G2**) were prepared through multistep syntheses, following previously reported procedures (see the ESI†). Both precursors were designed to include a terminal alkyne moiety, enabling the functionalization of the final monomer *via* Cu(I)-catalyzed 1,3-dipolar cycloaddition (azide–alkyne click chemistry). This approach, previously utilized by our group and others for similar semiconducting polymer systems, was selected for its efficiency and versatility and the minimal formation of undesirable side products.[40,41] In addition, 1,2,3-triazoles are widely recognized as electronically neutral linkers that do not significantly disrupt the conjugation pathway when used as modular spacers in conjugated polymers, introducing minimal steric or electronic impact beyond their role in enabling side chain attachment. Using this strategy, monomers **DPP-G1** and **DPP-G2** were synthesized *via* reacting 5-bis(6-azidohexyl)-3,6-bis(5-bromothiophen-2-yl)-2,5-dihydropyrrolo[3,4-*c*]pyrrole-1,4-dione with alkyne-terminated precursors **G1** and **G2** *via* azide–alkyne click chemistry, affording **DPP-G1** (96%) and **DPP-G2** (66%). These monomers were subsequently co-polymerized through Stille polycondensation with two selected π-conjugated donors: bithiophene (BT) and thienothiophene (TT). Both donors are known to provide good charge transport properties in related conjugated polymer systems.[42–44] Notably, TT, with its fused thiophene rings, typically leads to polymers with higher crystallinity compared to BT,

which features a rotatable bond between the two thiophene units.[42,45] This difference in crystallinity is particularly intriguing when combined with dendronized side chains, providing a valuable opportunity to study the interplay between polymer chain design and the mechanical and electronic properties of these materials. Upon synthesis, the resulting polymers **P(G1-DPP-BT)**, **P(G2-DPP-BT)**, **P(G1-DPP-TT)**, and **P(G2-DPP-TT)** were purified through successive Soxhlet extraction in methanol, acetone, and hexanes and were collected in chloroform, followed by precipitation in methanol. The structure and purity of the polymers were confirmed *via* nuclear magnetic resonance spectroscopy and Fourier-transform infrared (FT-IR) spectroscopy (ESI† and Fig. S1).

Following purification, the new polymers were characterized using various techniques to probe the physical properties. The results are summarized in Table 1. First, size-exclusion chromatography was used to evaluate molecular weights and dispersity. **P(G1-DPP-BT)** was found to have a lower molecular weight (22 kDa) compared to **P(G1-DPP-TT)**, which exhibited a significantly higher molecular weight of 96 kDa. In contrast, both generation 2 semiconducting polymers displayed similar molecular weights of approximately 50 kDa. This can be potentially attributed to solubility differences between the growing polymer chains, with **P(G1-DPP-BT)** chains possibly reaching their solubility limit earlier than their thienothiophene analogue, **P(G1-DPP-TT)**, thereby restricting chain growth and leading to a lower molecular weight. Interestingly, the similar molecular weights observed for **P(G2-DPP-BT)** and **P(G2-DPP-TT)** can potentially indicate that the dendritic architecture imposes steric or solubility constraints that inherently limit chain extension, effectively normalizing molecular weights regardless of the monomer structure. The energy levels of the polymers were measured using cyclic voltammetry (Fig. S2, ESI†). All polymers showed HOMO levels ranging between −5.2 and −5.5 eV and LUMO levels between −3.9 and −4.0, which agrees with previous results obtained on similar polymer systems.[46] Both **G1** and **G2** side chains showed very little influence on the bandgap and energy levels. Thermal decomposition temperatures were evaluated using thermogravimetric analysis at a 5% weight loss (Fig. S3, ESI†). All polymers showed high stability, with all polymers decomposing over 330 °C.

Following the initial characterization of the physical properties of the new semiconducting materials, UV-vis spectroscopy was performed in the solution and solid states to gain insight into the influence of the dendritic moieties and different backbone donating units on the optoelectronic properties. Notably, information about the molecular aggregation of polymer chains can be obtained by comparing the ratios of the 0-0 and 0-1 vibrational peaks, which correspond to aggregated and non-aggregated species, respectively.[28] All polymers exhibited typical absorption spectra for DPP-based conjugated polymers, as shown in Fig. 2 and Table 1.[28,47,48] The incorporation of generation 1 and 2 side chains significantly influenced the optical properties of the polymers in $CHCl_3$. **P(G1-DPP-BT)** exhibited absorption bands centered at λ = 434 and 789 nm, while **P(G2-DPP-BT)** exhibited absorption bands centered at λ = 426 and 777 nm, respectively, which can be attributed to the π–π* transitions and donor–acceptor charge transfer vibrations, respectively. Similarly, **P(G1-DPP-TT)** and **P(G2-DPP-TT)** exhibit π–π* transitions at λ = 420 and 412 nm, respectively, while their donor–acceptor charge transfer vibrations appear at λ = 833 and 810 nm, respectively. The redshift between the BT and TT in the solution state can be associated with an increased effective conjugation when thienothiophene is used as a donor due to its planarity and rigidity, which has been previously observed in related systems.[49] The resulting blueshifts between **G1** and **G2** for the polymers can be attributed to the decrease in aggregation properties in solution, likely due to the bulk of the side chain. In the solid state, polymer chain aggregation differed notably, as λ_{max} for all four polymers increased by 20–40 nm for their donor–acceptor vibrations compared to their solution-state absorptions. Interestingly, all polymers, except for **P(G1-DPP-BT)**, exhibited similar aggregation behaviors in solution, showing an overall decrease in aggregation in the solid state in comparison to the solution state. In the solid state, both **P(G1-DPP-BT)** and **P(G2-DPP-BT)** were shown to have a similar 0-0/0-1 peak ratio, attributed to the relative minor difference in aggregation. In contrast, **P(G1-DPP-TT)** and **P(G2-DPP-TT)** differed significantly in their solid-state aggregation properties, with **P(G1-DPP-TT)** displaying a much higher 0-0/0-1 peak ratio than **P(G2-DPP-TT)**, indicating that **P(G1-DPP-TT)** aggregates more in the solid state than **P(G2-DPP-TT)**. While molecular weight (M_n) effects cannot be ruled out, these findings suggest that increasing the side chain size leads to a significant reduction in solid-state aggregation, likely due to the increased steric bulk from **G1** and **G2**. Notably, **P(G1-DPP-TT)** shows minimal change

Table 1 Molecular weight, polydispersity, optical properties, energy levels and decomposition temperatures of DPP-based polymers **P(G1-DPP-BT)**, **P(G2-DPP-BT)**, **P(G1-DPP-TT)**, and **P(G2-DPP-TT)**

Polymer	M_n[a] (kDa)	M_w[a] (kDa)	$Đ$[b]	$\lambda_{max(soln)}$[c]	$\lambda_{max(film)}$[c]	E_g^{opt}[d] (eV)	HOMO[e] (eV)	LUMO[f] (eV)	T_d[g] (°C)
P(G1-DPP-BT)	22.3	25.6	1.2	789	822	1.33	−5.2	−3.9	336
P(G2-DPP-BT)	50.2	61.2	1.2	777	822	1.33	−5.5	−4.0	333
P(G1-DPP-TT)	96.5	155.5	1.6	833	854	1.37	−5.3	−3.9	337
P(G2-DPP-TT)	51.1	72.6	1.4	810	841	1.37	−5.3	−3.9	360

[a] Number-average molecular weight and weight-average molecular weight estimated by high-temperature gel permeation chromatography in 1,2,4-trichlorobenzene at 140 °C using polystyrene as the standard. [b] Dispersity defined as M_w/M_n. [c] Absorption maxima determined in solution (2.5×10^{-4} g mL^{-1} in $CHCl_3$) and the spin-coated thin film. [d] Calculated using the following equation: gap = 1240/λ_{onset} of the polymer film. [e] Calculated from cyclic voltammetry (potentials *vs.* Ag/AgCl) using 0.1 M $TBAPF_6$ in CH_3CN as an electrolyte. [f] Estimated from the calculated E_g^{opt} and HOMO. [g] Determined from thermogravimetric analysis (TGA) at a 5% weight loss.

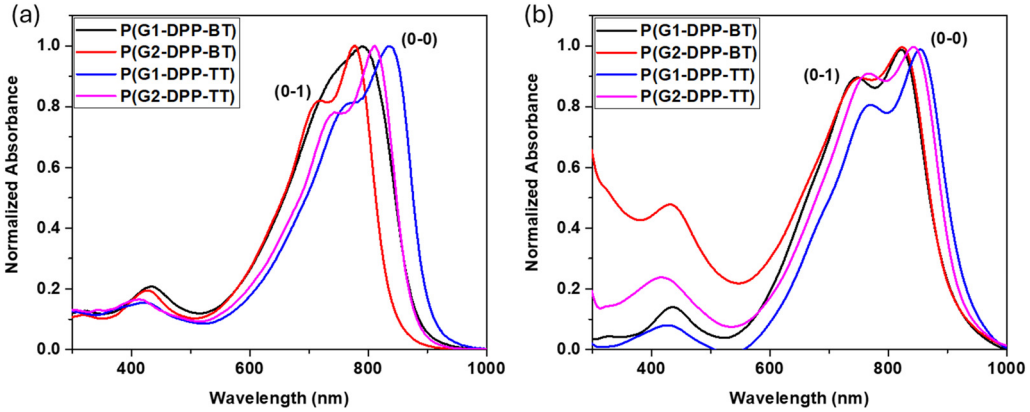

Fig. 2 Optical properties of the semiconducting polymers with poly(benzyl ether) side chains. UV-Vis spectra of **P(G1-DPP-BT)**, **P(G2-DPP-BT)**, **P(G1-DPP-TT)**, and **P(G2-DPP-TT)** in (a) solution in $CHCl_3$ and (b) thin film after thermal annealing at 150 °C for 1 hour.

between its solution and solid-state UV-vis spectra, a behavior not observed for the other polymers. This suggests relatively weaker interchain aggregation or a more planar conformation already present in solution, which could reduce the need for substantial reorganization during film formation and potentially benefit charge transport in devices.

Thermomechanical and thin film morphological properties of DPP polymers

To further investigate the nanoscale morphology of the new dendronized polymers, atomic force microscopy (AFM) was performed on thin films of **P(G1-DPP-BT)**, **P(G2-DPP-BT)**, **P(G1-DPP-TT)**, and **P(G2-DPP-TT)**. To replicate conditions typically used in the fabrication of organic field-effect transistors (OFETs), polymer thin films were prepared by spin-coating chlorobenzene-prepared polymer solutions onto an OTS-functionalized SiO_2 substrate, followed by thermal annealing at 150 °C for 1 hour. The results are summarized in Fig. 3. Notably, increasing the generation of the side chains on the DPP-polymer backbone led to a progressive decrease in surface roughness in both the BT and TT series. For example, **P(G1-DPP-BT)**, which features a generation 1 side chain, exhibited a root-mean-square (RMS) surface roughness of 5.0 nm. Upon increasing the side chain generation to **G2** in **P(G2-DPP-BT)**, the RMS roughness decreased to 3.6 nm. A similar trend was observed in the TT-series, where **P(G1-DPP-TT)** showed an RMS roughness of 5.8 nm, which dropped to 3.3 nm for **P(G2-DPP-TT)**. While these changes are relatively minor, the increasing size of the poly(benzyl ether) side chains can potentially lead to softening of the polymer film, influencing molecular aggregation and the overall smoothness of the films. This trend aligns well with observations from UV-vis spectroscopy.

To gain further insight into the morphological properties and characteristics of the polymers, grazing incidence wide-angle X-ray scattering (GIWAXS) was performed (Fig. 4a–d). The intermolecular lamellar spacing between adjacent polymer chains was determined from the 2D scattering patterns (Fig. 4e), while the out-of-plane π–π stacking distances of the conjugated backbones are summarized in Table S1 (ESI†). The corresponding 1D scattering vector profiles are shown in Fig. S4 (ESI†). The *d*-spacing for **P(G1-DPP-BT)** is 39.03 Å, increasing to 43.63 Å for **P(G2-DPP-BT)**. Similarly, **P(G1-DPP-TT)** exhibits a *d*-spacing of 39.03 Å, which increases to 42.45 Å for **P(G2-DPP-TT)**,

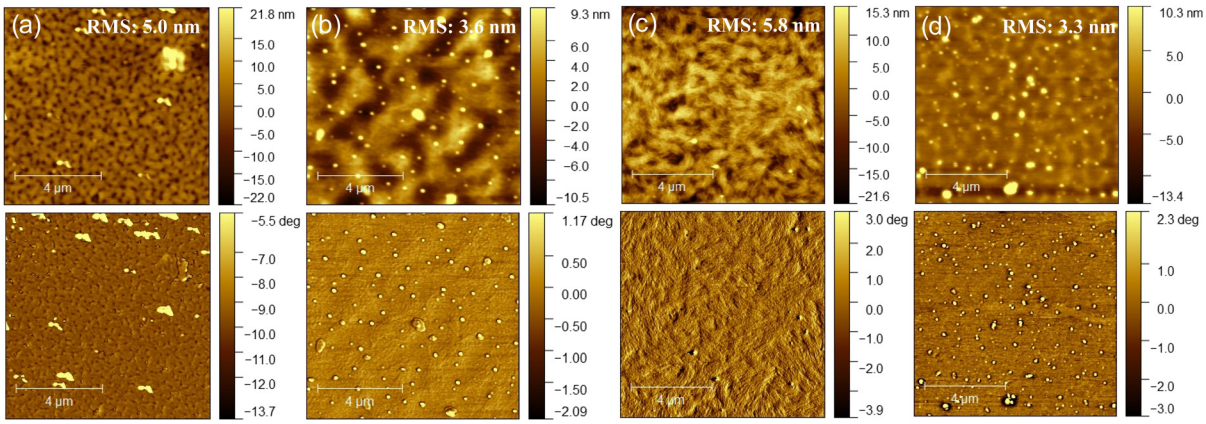

Fig. 3 Nanoscale morphology of the semiconducting polymers with poly(benzyl ether) dendrons. Atomic force microscopy (AFM) (a) height (top) and phase (bottom) images of **P(G1-DPP-BT)**; (b) height (top) and phase (bottom) images of **P(G2-DPP-BT)**, (c) height (top) and phase (bottom) images of **P(G1-DPP-TT)** and (d) height (top) and phase (bottom) images of **P(G2-DPP-TT)** after thermal annealing at 150 °C for 1 hour. The scale bar is 4 μm.

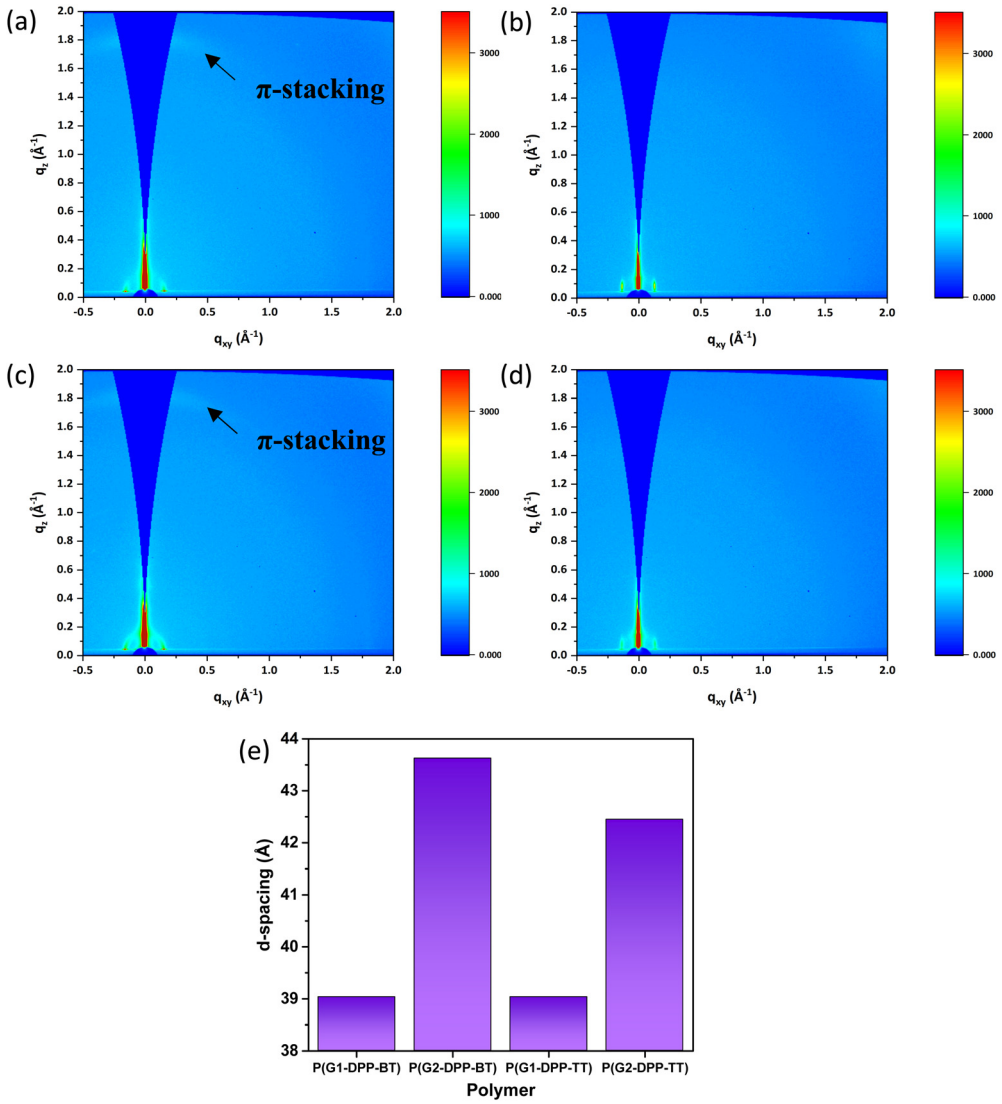

Fig. 4 Solid-state nanostructure in thin films investigated using X-ray scattering. Grazing incidence wide-angle X-ray scattering (GIWAXS) 2D patterns of (a) **P(G1-DPP-BT)**, (b) **P(G2-DPP-BT)**, (c) **P(G1-DPP-TT)**, and (d) **P(G2-DPP-TT)** and (e) lamellar spacing of **P(G1-DPP-BT)**, **P(G2-DPP-BT)**, **P(G1-DPP-TT)**, and **P(G2-DPP-TT)**, extracted from GIWAXS 2D patterns.

demonstrating that both the size and generation of the side chains significantly influence the molecular packing of these polymers. Notably, reducing the backbone length from BT to TT while increasing the planarity and rigidity resulted in no significant change in *d*-spacing within the **G1**-series, while there was a much more pronounced effect on the **G2** series, where the *d*-spacing for **P(G2-DPP-TT)** was 1.18 Å less than that of **P(G2-DPP-BT)**. The observed increase in *d*-spacing across generations can be closely correlated with the steric bulk and rotational freedom introduced by the **G1** and **G2** side chains. Higher-order reflections (100) were identified for all polymers and are presented in Fig. 4 and Fig. S4 and Table S1 (ESI†). Additionally, both generation 1 polymers exhibit some degree of π–π stacking in the out-of-plane direction, indicating the presence of both edge-on and face-on orientations relative to the OTS-functionalized substrate. This structural arrangement is further supported by the GIWAXS 2D profiles shown in Fig. 4.

To evaluate the mechanical properties of thin films and better understand the influence of both side chain generation and backbone incorporation, quantitative nanomechanical mapping (AFM) was utilized. The corresponding force plots and quantitative nanomechanical data are presented in Fig. S5 (ESI†). The results shown in Fig. 5a demonstrate that **P(G1-DPP-BT)** has a Young's modulus of 1560 MPa, which significantly decreases with increasing side chain size, as seen in **P(G2-DPP-BT)** having a modulus of 906 MPa. This suggests that larger side chains soften the polymer, likely due to an increase in the amorphous content and a reduction in molecular aggregation. A similar trend is observed when comparing **P(G1-DPP-TT)** (2698 MPa) to **P(G2-DPP-TT)** (2266 MPa). While this trend is consistent across the polymer series, the bithiophene-based polymers exhibit distinctly lower Young's moduli compared to their thienothiophene counterparts. This may be attributed to the effect from the backbone, as previous studies have shown

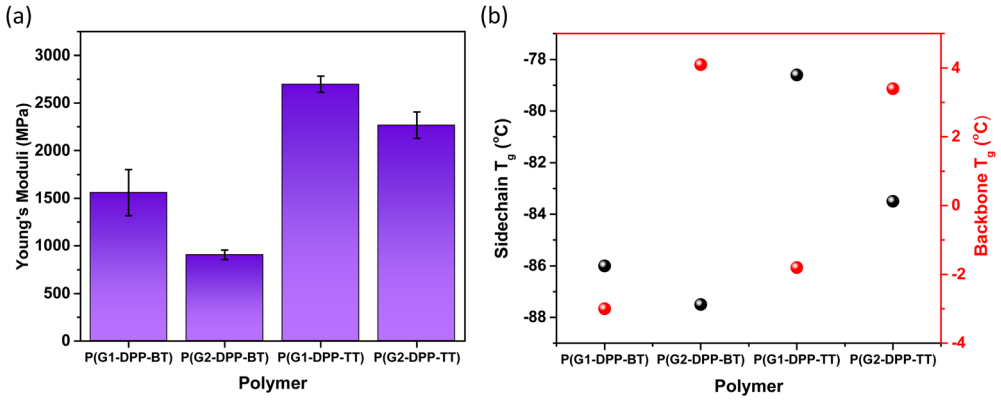

Fig. 5 Thermomechanical properties of the semiconducting polymers with poly(benzyl ether) dendrons. (a) Young's moduli of **P(G1-DPP-BT)**, **P(G2-DPP-BT)**, **P(G1-DPP-TT)**, and **P(G2-DPP-TT)** from quantitative nanomechanical mapping (AFM) and (b) backbone (red) and side chain (black) glass transition temperatures (T_g) determined through dynamic mechanical analysis (DMA).

that isolated thiophenes typically have lower elastic moduli compared to rigid, fused thiophene backbones. The increased stiffness and planarity of fused thiophenes often result in a higher T_g, contributing to the higher modulus observed in the thienothiophene series. These findings align with previous reports that bulky side chains reduce stiffness and enhance the softness of conjugated polymers, while rigid π-conjugated backbones increase stiffness and modulus. The observed decrease in Young's modulus with increasing side chain content highlights exciting potential for developing flexible and conformable technologies. By strategically tuning the size and intrinsic softness of side chains in conjugated polymers, it is possible to design materials with precisely controlled mechanical properties, enabling enhanced softness, stretchability, and flexibility.

The thermomechanical properties of the new dendron-bearing semiconducting polymers were further investigated using dynamic mechanical analysis (Fig. 5b and Fig. S6, ESI†). The detailed sample preparation procedures are described in the ESI.† Briefly, the polymers were drop-cast onto a meshed glass-fiber substrate as previously reported and dried overnight.[45] To avoid artifacts and erase the thermal history of the sample, the polymers were subjected to a full heating–cooling cycle prior to analysis. The side chain T_g values are determined from the loss modulus, while the backbone T_g values are extracted from the tan δ curve. Previous reports indicate that the branched, alkyl side chain transitions typically occur at lower temperatures, at approximately −50 °C in DPP-based polymers, whereas the backbone transitions for DPP-based polymers are typically observed around 0 °C.[45] In the current system, we found that as the side chain size increases and becomes increasingly soft across successive generations, the temperature range of the side chain transitions narrows and decreases drastically. Specifically, as the side chain generation increases from **G1** to **G2** for both donor series, the T_g is reduced for both the bithiophene and thienothiophene series to approximately −86 °C to −87 °C for **P(G1-DPP-BT)** and **P(G2-DPP-BT)**, while the side chain transitions for **P(G1-DPP-TT)** and **P(G2-DPP-TT)** are approximately −79 °C and −83 °C, respectively. A similar trend is observed for the backbone transitions, where increasing side chain bulk results in a higher backbone T_g for both the **G1** and **G2** series. There is a noticeable increase in the backbone T_g of the BT series when increasing the side chain generation from **G1** to **G2**, notably, from −3 to 4 °C. A similar trend was observed in the TT series, where the T_g occurs at −2 °C in **G1** and increases to 3 °C for **G2**. This result confirms that increasing the bulkiness of the side chain can lead to lower T_g for side chain transitions and an increase in backbone transitions.

The fabrication details and testing procedures for the prepared OFET devices are detailed in the ESI.† Briefly, all polymers were dissolved in anhydrous chlorobenzene (5 mg mL^{-1}) and stirred for 1 hour at 80 °C. The solution was then spin-coated onto an OTS-functionalized, bottom-gate top-contact (BGTC) silicon substrate. Mobilities were extracted by linear fitting of the $I_{DS}^{1/2}$ *vs.* V_{GS} transfer curves in the saturation regime, using the following equation: $I_{DS(sat)} = (WC/2L)\mu_{sat}(V_G - V_{th})^2$. The results obtained for all polymers are summarized in Fig. 6, with transfer and output characteristic curves in Fig. 6 and Fig. S7 and S8 (ESI†), respectively. All polymers tested showed typical transfer and output characteristics, except **P(G2-DPP-BT),** which showed non-ideal output characteristics and lower device yield (50%). **P(G1-DPP-BT)** and **P(G1-DPP-TT)** exhibited charge carrier mobilities comparable to those of other semiconducting polymers with aliphatic side chains. Among the new polymers tested, both generation 1 side chain bearing polymers showed good charge mobility. **P(G1-DPP-TT)** showed the highest performance, with an average mobility of 2.61 × 10^{-3} cm^2 V^{-1} s^{-1}, along with an on/off current ratio of 10^3 and an average threshold voltage of −18.7 V. In comparison, **P(G1-DPP-BT)** exhibited an average hole mobility of 6.03 × 10^{-4} cm^2 V^{-1} s^{-1}, a higher on/off current ratio of 10^4, and an average threshold voltage of −9.7 V. Upon increasing the side chain size from **G1** to **G2**, a significant decline in charge carrier mobility was observed. **P(G2-DPP-BT)** exhibited a charge carrier mobility of 4.39 × 10^{-4} cm^2 V^{-1} s^{-1}, an on/off current ratio of 10^1, and an average threshold voltage of −29.7 V, while also demonstrating non-ideal device behavior. The mobility of

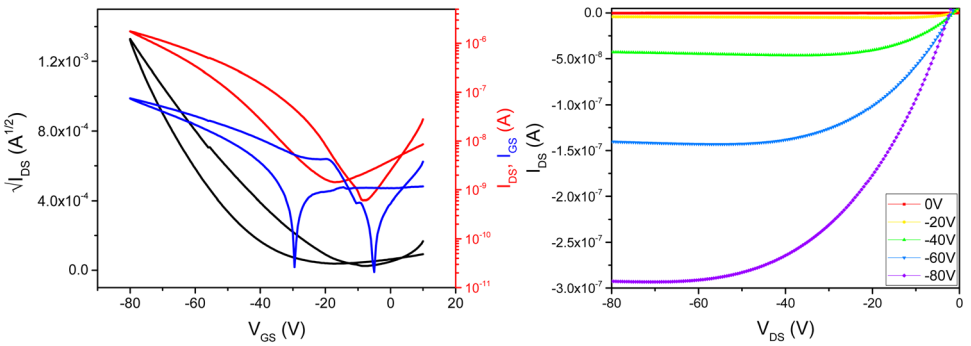

P(G1-DPP-BT)	Chlorobenzene	$6.03x10^{-4} \pm 2.58x10^{-4}/1.48x10^{-3}$	10^4	-9.7
P(G2-DPP-BT)	Chlorobenzene	$4.39x10^{-4} \pm 3.53x10^{-4}/1.31x10^{-3}$	10^1	-29.7
P(G1-DPP-TT)	Chlorobenzene	$2.61x10^{-3} \pm 8.54x10^{-4}/3.91x10^{-3}$	10^3	-18.7
P(G2-DPP-TT)	Chlorobenzene	$5.81x10^{-6} \pm 1.5x10^{-6}/8.34x10^{-6}$	10^3	-17.9

* Device mobilities, ON/OFF ratios and threshold voltages have been averaged from a minimum of 10 or more devices for each polymer. Each device was fabricated from the same batch for each polymer.

Fig. 6 Electronic properties of the semiconducting polymers with poly(benzyl ether) dendrons as measured using organic field-effect transistors. Representative transfer (top left) and output characteristic (top right) curves of **P(G1-DPP-TT)**, with average and maximum hole mobilities (μ_h^{ave}/μ_h^{max}), threshold voltages (V_{th}), and I_{on}/I_{off} current ratios for OFETs fabricated from semiconducting polymers (bottom). Device mobilities, threshold voltages, and I_{on}/I_{off} ratios have been averaged from a minimum of 10 or more devices for each polymer. Each device was fabricated from the same batch for each polymer.

P(G2-DPP-TT) decreased even more substantially to an average of 5.81×10^{-6} cm^2 V^{-1} s^{-1}, although it displayed typical output characteristics. This overall reduced performance can be attributed primarily to the structural effects introduced *via* side chain engineering. While the bulkier generation 2 poly(benzyl ether) side chains improve solubility and processability, they also introduce greater steric hindrance and rotational freedom, which can disrupt the conjugation length, hinder molecular packing, and impair charge transport pathways. In the case of **P(G2-DPP-TT)**, the mobility decline is particularly pronounced. This may arise from the interplay between the bulky **G2** side chains and the more planar backbone of the DPP-TT unit. The thienothiophene-based backbone generally favors stronger π–π stacking and crystallinity in the absence of steric disruption. However, the introduction of large side chains likely exacerbates steric congestion around this otherwise planar backbone, not only impeding π-stacking more severely than in **P(G2-DPP-BT)** but also potentially creating greater torsional disorder and severely limiting charge percolation pathways.

The observed charge carrier mobility trends align closely with the results obtained by GIWAXS; the decrease in mobility in OFETs corresponds to reduced crystallinity and increased π-stacking and lamellar *d*-spacing distances. **P(G1-DPP-TT)** shows the highest mobility, consistent with its tighter π-stacking (3.48 Å) and pronounced high-order (100) reflections, potentially indicative of a higher degree of crystallinity. This finding is in line with previous studies demonstrating that enhanced π-stacking and interdigitation promote charge carrier mobility.[35,50] In contrast, the increased π-stacking and lamellar distances in **P(G2-DPP-BT)** and **P(G2-DPP-TT)** are correlated with reduced mobility and more negative threshold voltages. This decline reflects less efficient intra- and intermolecular charge transport due to the bulkier side chains, which reduce crystalline order, increase amorphous content, and compromise polymer packing efficiency in the thin films.

Conclusions

In conclusion, a new series of diketopyrrolopyrrole-based (DPP) semiconducting polymers were prepared containing two generations of poly(benzyl ethers) incorporated by a macromonomer approach *via* Cu(I)-catalyzed 1,3-dipolar cycloaddition. In addition, the donor unit of the semiconducting polymers was varied to understand its influence. The resulting conjugated polymers were shown to become increasingly smooth as the side chain generation increased from **G1** to **G2**, indicating that large side chains were able to create a smoother surface *via* AFM. The polymers were also shown to possess high order reflections *via* GIWAXS for both generations of poly(benzyl ether) polymers, where generation 2 had a significant reduction in the overall crystallinity and loss of high order reflections. Quantitative nanomechanical mapping was used to investigate how the side chains influenced and affected the mechanical properties of thin films. Interestingly, upon increasing the size of the side chain in the polymer there was a significant decrease in the Young's modulus for each polymer, with **P(G2-DPP-BT)** having the lowest modulus of 906 MPa. To get a better understanding of the thermomechanical properties and how the side chain influenced them, dynamic mechanical analysis was utilized. In general, as the side chain increased in size for each polymer, the side chain T_g decreased and the backbone T_g increased. Bottom-gate top-contact organic field effect transistors were fabricated with all 4 polymers to analyze their potential for use in organic printable electronics. **P(G1-DPP-TT)** achieved the highest average mobility at

2.61×10^{-3} cm^2 V^{-1} s^{-1}, with **P(G1-DPP-BT)** decreasing slightly, averaging 6.03×10^{-4} cm^2 V^{-1} s^{-1}. Increasing the poly(benzyl ether) side chains to generation 2 significantly altered the performance characteristics of polymers, with the average mobility dropping to 5.81×10^{-6} cm^2 V^{-1} s^{-1} for **P(G2-DPP-TT)** and 4.39×10^{-4} cm^2 V^{-1} s^{-1} for **P(G2-DPP-BT)**, with non-ideal performance characteristics. These results confirm the potential of introducing bulky side chains to create softer conjugated polymers for use in organic electronics. However, careful design consideration is imperative, as bulkier side chains can disrupt thin film morphology and molecular packing, and hinder electronic performance. Overall, this work highlights the importance of balancing mechanical flexibility and charge transport to advance the design of next-generation semiconducting polymers.

Author contributions

All authors contributed to the manuscript. All authors have given approval to the final version of the manuscript.

Conflicts of interest

The authors declare no conflict of interest.

Data availability

The data supporting this article have been included as part of the ESI.†

Acknowledgements

This work was supported by NSERC through Discovery Grants (RGPIN-2022-04428) and the NSERC Green Electronics Network (GreEN) (NETGP 508526-17). S. R.-G. thanks the Canadian Fund for Innovation (CFI) for supporting the infrastructure used in this work. Y.-C. C. acknowledges financial support from the National Science and Technology Council in Taiwan (NSTC 113-2124-M-011-002).

References

1 S. Wang, J. Y. Oh, J. Xu, H. Tran and Z. Bao, *Acc. Chem. Res.*, 2018, **51**, 1033–1045.
2 L. V. Kayser and D. J. Lipomi, *Adv. Mater.*, 2019, **31**, 1806133.
3 M. L. Hammock, A. Chortos, B. C. K. Tee, J. B. H. Tok and Z. Bao, *Adv. Mater.*, 2013, **25**, 5997–6038.
4 P. B. J. St. Onge, M. U. Ocheje, M. Selivanova and S. Rondeau-Gagné, *Chem. Rec.*, 2019, **19**, 1008–1027.
5 M. Mooney, A. Nyayachavadi and S. Rondeau-Gagné, *J. Mater. Chem. C*, 2020, **8**, 14645–14664.
6 Y. Zhan, Y. Mei and L. Zheng, *J. Mater. Chem. C*, 2014, **2**, 1220–1232.
7 Q. Shi, B. Dong, T. He, Z. Sun, J. Zhu, Z. Zhang and C. Lee, *InfoMat*, 2020, **2**, 1131–1162.
8 J. Shi, S. Liu, L. Zhang, B. Yang, L. Shu, Y. Yang, M. Ren, Y. Wang, J. Chen, W. Chen, Y. Chai and X. Tao, *Adv. Mater.*, 2020, **32**, 1901958.
9 E. S. Hosseini, S. Dervin, P. Ganguly and R. Dahiya, *ACS Appl. Bio Mater.*, 2021, **4**, 163–194.
10 Y. Khan, A. Thielens, S. Muin, J. Ting, C. Baumbauer and A. C. Arias, *Adv. Mater.*, 2020, **32**, 1905279.
11 Y. S. Rim, S. H. Bae, H. Chen, N. De Marco and Y. Yang, *Adv. Mater.*, 2016, **28**, 4415–4440.
12 X. Xu, Y. Zhao and Y. Liu, *Small*, 2023, **19**, 2206309.
13 C. Wang, Y. J. Kim, A. Vriza, R. Batra, A. Baskaran, N. Shan, N. Li, P. Darancet, L. Ward, Y. Liu, M. K. Y. Chan, S. K. R. S. Sankaranarayanan, H. C. Fry, C. S. Miller, H. Chan and J. Xu, *Nat. Commun.*, 2025, **16**, 1498.
14 Y. Bonnassieux, C. J. Brabec, Y. Cao, T. B. Carmichael, M. L. Chabinyc, K. T. Cheng, G. Cho, A. Chung, C. L. Cobb, A. Distler, H. J. Egelhaaf, G. Grau, X. Guo, G. Haghiashtiani, T. C. Huang, M. M. Hussain, B. Iniguez, T. M. Lee, L. Li, Y. Ma, D. Ma, M. C. McAlpine, T. N. Ng, R. Österbacka, S. N. Patel, J. Peng, H. Peng, J. Rivnay, L. Shao, D. Steingart, R. A. Street, V. Subramanian, L. Torsi and Y. Wu, *Flexible Printed Electron.*, 2021, **6**, 023001.
15 C. Liao, M. Zhang, M. Y. Yao, T. Hua, L. Li and F. Yan, *Adv. Mater.*, 2015, **27**, 7493–7527.
16 A. Nyayachavadi, C. Wang, A. Vriza, Y. Wang, G. Ma, M. Mooney, G. T. Mason, A. Hu, Y. Liu, X. Gu, H. Chan, J. Xu and S. Rondeau-Gagné, *Adv. Funct. Mater.*, 2024, **34**, 2403612.
17 H. Sirringhaus, *Adv. Mater.*, 2014, **26**, 1319–1335.
18 Y. Olivier, D. Niedzialek, V. Lemaur, W. Pisula, K. Müllen, U. Koldemir, J. R. Reynolds, R. Lazzaroni, J. Cornil and D. Beljonne, *Adv. Mater.*, 2014, **26**, 2119–2136.
19 Y. Luo, M. R. Abidian, J. H. Ahn, D. Akinwande, A. M. Andrews, M. Antonietti, Z. Bao, M. Berggren, C. A. Berkey, C. J. Bettinger, J. Chen, P. Chen, W. Cheng, X. Cheng, S. J. Choi, A. Chortos, C. Dagdeviren, R. H. Dauskardt, C. A. Di, M. D. Dickey, X. Duan, A. Facchetti, Z. Fan, Y. Fang, J. Feng, X. Feng, H. Gao, W. Gao, X. Gong, C. F. Guo, X. Guo, M. C. Hartel, Z. He, J. S. Ho, Y. Hu, Q. Huang, Y. Huang, F. Huo, M. M. Hussain, A. Javey, U. Jeong, C. Jiang, X. Jiang, J. Kang, D. Karnaushenko, A. Khademhosseini, D. H. Kim, I. D. Kim, D. Kireev, L. Kong, C. Lee, N. E. Lee, P. S. Lee, T. W. Lee, F. Li, J. Li, C. Liang, C. T. Lim, Y. Lin, D. J. Lipomi, J. Liu, K. Liu, N. Liu, R. Liu, Y. Liu, Y. Liu, Z. Liu, Z. Liu, X. J. Loh, N. Lu, Z. Lv, S. Magdassi, G. G. Malliaras, N. Matsuhisa, A. Nathan, S. Niu, J. Pan, C. Pang, Q. Pei, H. Peng, D. Qi, H. Ren, J. A. Rogers, A. Rowe, O. G. Schmidt, T. Sekitani, D. G. Seo, G. Shen, X. Sheng, Q. Shi, T. Someya, Y. Song, E. Stavrinidou, M. Su, X. Sun, K. Takei, X. M. Tao, B. C. K. Tee, A. V. Y. Thean, T. Q. Trung, C. Wan, H. Wang, J. Wang, M. Wang, S. Wang, T. Wang, Z. L. Wang, P. S. Weiss, H. Wen, S. Xu, T. Xu, H. Yan, X. Yan, H. Yang, L. Yang, S. Yang, L. Yin, C. Yu, G. Yu, J. Yu, S. H. Yu, X. Yu, E. Zamburg, H. Zhang, X. Zhang, X. Zhang, X. Zhang, Y. Zhang, Y. Zhang, S. Zhao, X. Zhao, Y. Zheng,

Y. Q. Zheng, Z. Zheng, T. Zhou, B. Zhu, M. Zhu, R. Zhu, Y. Zhu, Y. Zhu, G. Zou and X. Chen, *ACS Nano*, 2023, **17**, 5211–5295.

20 J. Kang, J. B. H. Tok and Z. Bao, *Nat. Electron.*, 2019, **2**, 144–150.

21 J. Mei and Z. Bao, *Chem. Mater.*, 2014, **26**, 604–615.

22 S. Zhang, A. Alesadi, M. Selivanova, Z. Cao, Z. Qian, S. Luo, L. Galuska, C. Teh, M. U. Ocheje, G. T. Mason, P. B. J. St. Onge, D. Zhou, S. Rondeau-Gagné, W. Xia and X. Gu, *Adv. Funct. Mater.*, 2020, **30**, 2002221.

23 J. A. Rogers and Z. Bao, *J. Polym. Sci., Part A: Polym. Chem.*, 2002, **40**, 3327–3334.

24 C. S. Buga and J. C. Viana, *Adv. Mater. Technol.*, 2021, **6**, 2001016.

25 K. S. Park, J. J. Kwok, P. Kafle and Y. Diao, *Chem. Mater.*, 2021, **33**, 469–498.

26 X. Guo, M. Baumgarten and K. Müllen, *Prog. Polym. Sci.*, 2013, **38**, 1832–1908.

27 C. Lu, W. Y. Lee, X. Gu, J. Xu, H. H. Chou, H. Yan, Y. C. Chiu, M. He, J. R. Matthews, W. Niu, J. B. H. Tok, M. F. Toney, W. C. Chen and Z. Bao, *Adv. Electron. Mater.*, 2017, **3**, 1600311.

28 B. C. Schroeder, T. Kurosawa, T. Fu, Y. C. Chiu, J. Mun, G. J. N. Wang, X. Gu, L. Shaw, J. W. E. Kneller, T. Kreouzis, M. F. Toney and Z. Bao, *Adv. Funct. Mater.*, 2017, **27**, 1701973.

29 B. Meng, J. Liu and L. Wang, *Polym. Chem.*, 2020, **11**, 1261–1270.

30 M. Mooney, Y. Wang, A. Nyayachavadi, S. Zhang, X. Gu and S. Rondeau-Gagné, *ACS Appl. Mater. Interfaces*, 2021, **13**, 25175–25185.

31 M. Mooney, Y. Wang, E. Iakovidis, X. Gu and S. Rondeau-Gagné, *ACS Appl. Electron. Mater.*, 2022, **4**, 1381–1390.

32 A. Nyayachavadi, G. T. Mason, M. Nazir Tahir, M. U. Ocheje and S. Rondeau-Gagné, *Langmuir*, 2018, **34**, 12126–12136.

33 A. Nyayachavadi, A. K. Sur, P. Kulatunga, Y. Wang, T. C. Gomes, M. Mooney, G. T. Mason, A. Hu, X. Gu and S. Rondeau-Gagné, *Chem. Mater.*, 2023, **35**, 9682–9691.

34 Y. C. Chiang, H. C. Wu, H. F. Wen, C. C. Hung, C. W. Hong, C. C. Kuo, T. Higashihara and W. C. Chen, *Macromolecules*, 2019, **52**, 4393–4404.

35 J. Mei, D. H. Kim, A. L. Ayzner, M. F. Toney and Z. Bao, *J. Am. Chem. Soc.*, 2011, **133**, 20130–20133.

36 H. C. Wu, C. C. Hung, C. W. Hong, H. S. Sun, J. T. Wang, G. Yamashita, T. Higashihara and W. C. Chen, *Macromolecules*, 2016, **49**, 8540–8548.

37 Z. Bao, K. R. Amundson and A. J. Lovinger, *Macromolecules*, 1998, **31**, 8647–8649.

38 J. J. Apperloo, R. A. J. Janssen, P. R. L. Malenfant, L. Groenendaal and J. M. J. Fréchet, *J. Am. Chem. Soc.*, 2000, **122**, 7042–7051.

39 X. Xiao, Y. Wu, M. Sun, J. Zhou, Z. Bo, L. Li and C. Chan, *J. Polym. Sci., Part A: Polym. Chem.*, 2007, **46**, 574–584.

40 G. T. Mason, A. Nyayachavadi, M. Mooney, K. Schlingman and S. Rondeau-Gagné, *J. Polym. Sci.*, 2022, **60**, 590–601.

41 N. Li, Y. Dai, Y. Li, S. Dai, J. Strzalka, Q. Su, N. De Oliveira, Q. Zhang, P. B. J. St. Onge, S. Rondeau-Gagné, Y. Wang, X. Gu, J. Xu and S. Wang, *Matter*, 2021, **4**, 3015–3029.

42 X. Zhang, L. J. Richter, D. M. Delongchamp, R. J. Kline, M. R. Hammond, I. McCulloch, M. Heeney, R. S. Ashraf, J. N. Smith, T. D. Anthopoulos, B. Schroeder, Y. H. Geerts, D. A. Fischer and M. F. Toney, *J. Am. Chem. Soc.*, 2011, **133**, 15073–15084.

43 J. S. Lee, S. K. Son, S. Song, H. Kim, D. R. Lee, K. Kim, M. J. Ko, D. H. Choi, B. S. Kim and J. H. Cho, *Chem. Mater.*, 2012, **24**, 1316–1323.

44 Y. Li, P. Sonar, S. P. Singh, M. S. Soh, M. Van Meurs and J. Tan, *J. Am. Chem. Soc.*, 2011, **133**, 2198–2204.

45 S. Zhang, M. U. Ocheje, L. Huang, L. Galuska, Z. Cao, S. Luo, Y. H. Cheng, D. Ehlenberg, R. B. Goodman, D. Zhou, Y. Liu, Y. C. Chiu, J. D. Azoulay, S. Rondeau-Gagné and X. Gu, *Adv. Electron. Mater.*, 2019, **5**, 1800899.

46 J. C. Bijleveld, A. P. Zoombelt, S. G. J. Mathijssen, M. M. Wienk, M. Turbiez, D. M. De Leeuw and R. A. J. Janssen, *J. Am. Chem. Soc.*, 2009, **131**, 16616–16617.

47 D. Liu, J. Mun, G. Chen, N. J. Schuster, W. Wang, Y. Zheng, S. Nikzad, J. C. Lai, Y. Wu, D. Zhong, Y. Lin, Y. Lei, Y. Chen, S. Gam, J. W. Chung, Y. Yun, J. B. H. Tok and Z. Bao, *J. Am. Chem. Soc.*, 2021, **143**, 11679–11689.

48 S. Chen, Y. Meng, Y. Li, B. Qu and D. Zhuo, *Opt. Mater.*, 2019, **88**, 500–507.

49 D. Venkateshvaran, M. Nikolka, A. Sadhanala, V. Lemaur, M. Zelazny, M. Kepa, M. Hurhangee, A. J. Kronemeijer, V. Pecunia, I. Nasrallah, I. Romanov, K. Broch, I. McCulloch, D. Emin, Y. Olivier, J. Cornil, D. Beljonne and H. Sirringhaus, *Nature*, 2014, **515**, 384–388.

50 Y. Lee, M. Shin, K. Thiyagarajan and U. Jeong, *Macromolecules*, 2016, **49**, 433–444.